Coherent description of the magnetic properties of SeCuO3 versus temperature and magnetic field

Xavier Rocquefelte, Mirta Herak, Atsushi Miyake, William Lafargue-Dit-Hauret, Helmuth Berger, Masashi Tokunaga, Andres Saúl

Coherent description of the magnetic properties of $SeCuO_3$ versus temperature and magnetic field

Xavier Rocquefelte,[1,*] Mirta Herak,[2] Atsushi Miyake,[3] William Lafargue-Dit-Hauret,[1] Helmuth Berger,[4] Masashi Tokunaga,[3] and Andres Saúl[5,†]

[1] *Univ Rennes, CNRS, ISCR (Institut des Sciences Chimiques de Rennes) UMR 6226, F-35000 Rennes, France*
[2] *Institute of Physics, Bijenička c. 46, HR-10000 Zagreb, Croatia*
[3] *Institute for Solid State Physics, The University of Tokyo, Kashiwa, Chiba 277-8581, Japan*
[4] *Institute of Physics, Ecole Polytechnique Fédérale de Lausanne (EPFL), CH-1015 Lausanne, Switzerland*
[5] *Aix Marseille Univ, CNRS, CINaM UMR 7325, Campus de Luminy Case 913, 13288 Marseille, France*

(Dated: February 9, 2023)

We report a combined theoretical and experimental investigation devoted to get deeper insights on the exotic magnetic properties of the low-dimensional $SeCuO_3$ system, for which the two inequivalent Cu(1) and Cu(2) sites show different quantum dynamics. First-principles calculations based on the density functional theory were performed to extract the magnetic exchange couplings. Briefly, we notably evidenced that i) the magnetic structure can be decomposed into two subsystems made by strongly antiferromagnetically (AFM) coupled Cu(1) singlet state dimers and weak AFM Cu(2) spin chains, and ii) weak ferromagnetic (FM) interactions between the two subsystems lead to magnetic frustration. The present model allows to reproduce both magnetic susceptibility and torque magnetometry measurements. In addition, high-magnetic field experiments and DMRG simulations evidenced a half-magnetization plateau at 40-45 T associated to the polarization of the Cu(2) spin-chains, while the Cu(1) dimers are expected to reach the triplet state at 210-220 T.

I. INTRODUCTION

Low-dimensionality often leads to intriguing and fascinating phenomena in condensed matter. When the structural dimension of materials is reduced, significant changes in properties may arise, resulting from the enhancement of thermal and quantum fluctuations. A wide variety of exotic magnetic properties has been reported for low-dimensional magnets, whether they are zero- (dimers, trimers, tetramers), one- (chains, ladders), or two-dimensional (planes) [1]. Among the zero-dimensional objects, the simplest non trivial case is the spin-1/2 dimer involved in a strong antiferromagnetic (AFM) exchange coupling which stabilizes the entity within the singlet ground state. Such strongly bounded dimers may sometimes be weakly coupled and form Bose-Einstein condensates (BEC) [2, 3].

In a large majority of low dimensional systems the magnetic structures (dimers, ladders, planes, chains, etc) correspond to structural units clearly recognizable in the crystallographic structure. The interesting cases are the "surprises", where the magnetic units as defined by the leading magnetic effective interactions do not strictly agree with the structural ones. For instance, both CsV_2O_5 and CuO compounds exhibit one-dimensional magnetic properties, while the topologies of the magnetic elements, *i.e.* V^{4+} and Cu^{2+} ions respectively, are zero-dimensional ($[V_2O_8]^{8-}$ dimers separated by $[VO_4]^{3-}$ non-magnetic bridging units) and three-dimensional [4, 5], respectively.

In this work we are interested in the monoclinic phase of $SeCuO_3$, where the magnetic Cu^{2+} ions form structural spin-1/2 tetramers [6–9]. This particularity has motivated a special interest to study quantum effects in this system [6–11]. For instance, magnetic susceptibility and torque magnetometry measurements evidenced that this compound shows an AFM long-range ordering up to $T_N = 8$ K, with an easy magnetization axis along the reciprocal $[\bar{1}01]$ ($[\bar{1}01]^*$) direction [6, 7]. Based on its crystallographic structure where Cu tetramers can be clearly recognized, a first tetramer magnetic model has been tentatively proposed to extract the magnetic phase diagram. Unfortunately, this model failed to retrieve the whole temperature dependence of the magnetic susceptibility, more specifically the low-temperature range. Furthermore, some studies concluded that the two symmetrically inequivalent Cu(1) and Cu(2) sites show different quantum dynamics [6, 8–10], which would be at the origin of the unusual magnetic properties of $SeCuO_3$. In parallel, high-field magnetization measurements showed the existence of a half-step magnetization plateau at 45 T [8], which supposedly emerges from the polarization of weakly coupled Cu(2) spins, while Cu(1) dimers remain in the singlet state. This new magnetic model was supported a few years later by inelastic neutron scattering, used to determine magnetic exchange couplings and demonstrate the simultaneous presence of magnon, triplon and spinon excitations [11].

In this paper, we report a combined theoretical and experimental investigation to study the magnetic properties of the $SeCuO_3$ system. The paper is organized as follows. In Section II we discuss the theoretical and experimental methods used in this work. In Section III A we present our estimation of the effective magnetic ex-

* xavier.rocquefelte@univ-rennes1.fr
† andres.saul@cnrs.fr

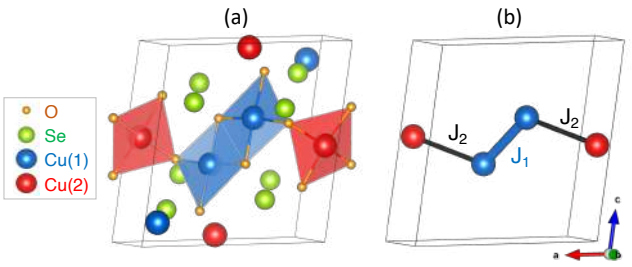

Figure 1. (a) Schematic representation of the crystallographic structure of $SeCuO_3$. The two inequivalent copper atoms Cu(1) and Cu(2) are respectively depicted by blue and red spheres. For the sake of clarity, the square-planar environments of the four copper atoms defining only one tetramer entity are shown. (b) Schematic representation of intra-tetramer exchange couplings, *i.e.* J_1 between Cu(1) sites and J_2 between Cu(1) and Cu(2) sites. (All crystal visualization in this paper were performed using VESTA [13]).

change interactions in this compound. In Section III B we present our magnetic susceptibility and torque measurements and in Section III C the results of our magnetization versus magnetic field experiments. Our study leads to the proposition of a magnetic model formed of weakly connected dimers and chains enabling to explain the experimental data for the whole range of temperature and magnetic field.

II. METHODOLOGY

A. $SeCuO_3$ structure

Among the four known phases of $SeCuO_3$[12], we focus herein on the monoclinic structure which crystallizes in the space group $P2_1/n$ (# 14), with lattice parameters: $a = 7.725(1)$ Å, $b = 8.241(1)$ Å, $c = 8.502(1)$ Å and $\beta = 99.16(2)°$. The unit cell (see Figure 1) contains two crystallographic inequivalent copper atoms, labelled Cu(1) and Cu(2). Each copper site is embedded within a highly distorted CuO_6 octahedron with elongated apical Cu-O bonds leading to square-planar CuO_4 environment (or *plaquette*). Structurally speaking, the atomic structure can be viewed as being formed by tetramers Cu(2)-Cu(1)-Cu(1)-Cu(2), separated by SeO_3E entities (E refers to a lone-pair). One tetramer unit is emphasized in Figure 1a. It consists in two Cu(1) O_4 plaquettes sharing edges forming a Cu(1)-Cu(1) dimer, and two corner-sharing Cu(2) O_4 plaquettes at each side of the Cu(1)-Cu(1) dimer.

B. Experimental details

Magnetic susceptibility was measured using Faraday method in applied magnetic field up to $\mu_0 H = 0.9$ T and in the temperature range $2 - 300$ K. Magnetic torque was measured using highly sensitive home-built torque magnetometer in the applied magnetic field up to $\mu_0 H = 0.8$ T in the temperature range $2 - 300$ K. The sensitivity of the magnetometer is 10^{-11} Nm.

Magnetization in pulsed-magnetic fields was measured using the conventional induction method, employing coaxial pick-up coils. Pulsed-magnetic fields up to 66 T with typical duration of ~ 11 ms were generated by using a pulse magnet installed at the International Mega-Gauss Science Laboratory at the Institute for Solid State Physics of the University of Tokyo.

C. Computational details

We performed density functional theory (DFT) calculations [14, 15] using the QUANTUM ESPRESSO code [16]. We considered the general-gradient approximation GGA-PBE parametrization [17] for the exchange-correlation term. The calculations were performed using ultrasoft pseudopotentials [18] with a plane-wave and charge density cutoff of 60 Ry and 400 Ry, respectively, and a 1×3×1 Monkhorst-Pack [19] grid for the first Brillouin zone sampling of the 2×1×2 160-atoms cell. We included an on-site Hubbard U_{eff} on the Cu atoms using the simplified method developed by Cococcioni and de Gironcoli [20] with a $U_{\text{eff}} = 10$ eV. For the DFT calculations the volume of the unit cell and internal coordinates were fully relaxed. The obtained optimized lattice parameters are $a = 7.7124$ Å, $b = 8.2380$ Å, $c = 8.4979$ Å, $\beta = 99.124°$.

To describe the magnetic properties of $SeCuO_3$, we have estimated the magnetic exchange interactions based on the following rotational invariant Heisenberg Hamiltonian:

$$\hat{H} = \hat{H}_0 + \sum_{i>j} J_{ij}\ \hat{S}_i \cdot \hat{S}_j, \qquad (1)$$

where $\hat{H}_0$ is the spin independent part of the Hamiltonian, J_{ij} the magnetic coupling between the magnetic sites i and j, and $\hat{S}_i$ and $\hat{S}_j$ are the related quantum $S = 1/2$ spin operators. The broken symmetry method [21, 22] has been used to calculate the effective exchange interactions J_{ij} [4, 23, 24]. The J_{ij} interaction between spins $\hat{S}_i$ and $\hat{S}_j$ can be evaluated from:

$$J_{ij} = E(\uparrow_i\uparrow_j) + E(\downarrow_i\downarrow_j) - E(\uparrow_i\downarrow_j) - E(\downarrow_i\uparrow_j) \qquad (2)$$

where $E(\sigma_i, \sigma_j)$ are the four spin configurations where the spins $\hat{S}_i$ and $\hat{S}_j$ can either take the values up ($\uparrow$) or down ($\downarrow$) while all the other spins are kept up. Hereafter, $J > 0$ indicates an antiferromagnetic (AFM) coupling, while $J < 0$ indicates a ferromagnetic (FM) coupling.

The high-field magnetization $M(\mathbf{H})$ has been simulated using the density-matrix renormalization-group (DMRG) method [25]. To represent the full magnetic

Table I. Magnetic exchange couplings determined from DFT calculations (labelled J^{th}) and compared to experimental data when available (labelled J^{exp}) [11]. For each J_{ij} interaction, the related Cu(i)-Cu(j) pair is specified between parenthesis. Experimental and optimized distances between copper sites are reported as d^{exp}_{Cu-Cu} and d^{th}_{Cu-Cu}, respectively.

J_{ij} (i,j)	d^{exp}_{Cu-Cu} (Å)	d^{th}_{Cu-Cu} (Å)	J^{th} (K)	J^{exp} (K)
J_1 (1,1)	3.039	3.036	270.0	308
J_2 (1,2)	3.199	3.191	-38.1	40[b]
J_3 (1,2)	3.395	3.397	-7.6	
J_4 (2,2)	3.474	3.467	0[a]	-2
J_5 (1,2)	4.219	4.212	-20.0	41[b]
J_6 (1,2)	4.752	4.750	-5.8[a]	
J_7 (2,2)	4.871	4.875	0[a]	
J_8 (1,2)	5.112	5.106	0.1	
J_9 (1,2)	5.179	5.170	-8.0	
J_{10} (2,2)	5.316	5.314	12.6	5
J_{11} (1,1)	5.532	5.526	26.4	
J_{12} (1,1)	5.804	5.802	0.3	
J_{13} (1,2)	5.881	5.878	0.9	
J_{14} (1,2)	6.046	6.045	0.8	
J_{15} (1,2)	6.066	6.063	1.4[a]	
J_{16} (2,2)	6.222	6.215	29.2	39

[a] J_4 and J_7 couplings cannot be separated within the supercell used in the DFT calculations, as for J_6 and J_{15} interactions.
[b] These values have been deduced from a perturbative analysis and are not directly extracted from the dispersion of the inelastic neutron scattering data.

model, we considered two Cu(2) spin-chains (dimension of one chain: n+1) and n Cu(1) dimers, with n = 10, 20 and 50, in order to check the convergency of the DMRG calculations, which have been compared to exact diagonalization calculations for the smaller n values.

III. RESULTS AND DISCUSSION

A. Magnetic exchange couplings

As aforementioned, despite the presence of clearly recognizable structural Cu tetramers in the crystallographic structure of $SeCuO_3$, recent magnetic torque measurements [10] have proposed the magnetic structure as based on two subsystems which involves, respectively, strongly coupled Cu(1) dimers and weakly coupled Cu(2) spins. To get a deeper insight on such models, we estimated all possible magnetic exchange interactions up to Cu-Cu distances of 6.2 Å (see Figure 2 and Table I), leading to a total of 16 J_{ij} couplings. For the sake of clarity, the Cu(1)-Cu(1) and Cu(2)-Cu(2) intrasublattice interactions are labelled (1,1) and (2,2), respectively, and the Cu(1)-Cu(2) intersublattice interactions are labelled (1,2).

The largest interaction, *i.e.* J_1 = 270 K, is ten times larger than the others and defines the strongly antiferromagnetically (AFM) coupled Cu(1)-Cu(1) dimers. A very good agreement is found with the experimental estimation from neutron scattering data (308 K). Among the two other (1,1) interactions, one is antiferromagnetic but significantly smaller, *i.e.* J_{11} = 26 K, and the other one (J_{12}) is zero. In conclusion, the Cu(1)-sublattice consists in weakly interacting AFM dimers, ($J_1/J_{11} > 10$) as shown in Figure 2a.

Among the four (2,2) intrasublattice interactions, only two have non-zero values and correspond to AFM couplings, *i.e.* J_{16} = 29 K and J_{10} = 13 K. A qualitative agreement is found with the neutron estimated values, which are 39 K and 5 K, respectively. In particular, both estimations suggest that the largest Cu(2)-Cu(2) coupling involves copper pairs separated by 6.2 Å, which leads to one-dimensional (1D) chains along the [10-1] direction. The other interaction (J_{10}) forms 1D chains along the [101] direction. The Cu(2) sublattice can then be viewed as a system of non frustrated AFM chains with intra-chain and inter-chain interactions J_{16} and J_{10} respectively (see Figure 2b).

We have also estimated 9 intersublattice interactions, labelled (1,2). Among them, four are negligible, *i.e.* smaller than 1.5 K (J_8, J_{13}, J_{14} and J_{15}). The others are ferromagnetic (FM), with two couplings which are significantly larger than the others, J_2 = -38 K and J_5 = -20 K. The related experimental values were not directly deduced from fitting the neutron dispersion data, but by performing a perturbative analysis of a four-site model [11]. It leads the authors to estimate the square values of J_2 and J_5 (see equation 2 of ref. [11]), and thus only their absolute values, *i.e.* 40 and 41 K, respectively.

Figure 2c shows these two FM intersublattice interactions, which connect the AFM Cu(2) chains (red sites) to the AFM Cu(1) dimers.

In summary, the image that arises from the present DFT calculations is the following (see Figure 7a). Firstly, it confirms that $SeCuO_3$ consists in two magnetic subsystems, *i.e.* weakly interacting AFM Cu(1) dimers and interacting AFM Cu(2) spin chains. Secondly, the intersublattice interactions are FM, leading to magnetic frustration which effectively decouples, at low temperature and magnetic field, the singlet AFM dimers to the chains.

B. Magnetic susceptibility and torque magnetometry results

In order to check the validity of our magnetic model based on the present DFT calculations, we reconsidered the modelling of the magnetic susceptibility data. To assess the effect of each type of magnetic interaction, we considered five different situations: i) isolated chains (hereafter labelled C), ii) weakly interacting chains (wC), iii) isolated dimers (D) and, iv) weakly interacting dimers (wD) and v) decoupled chains and dimers subsystems

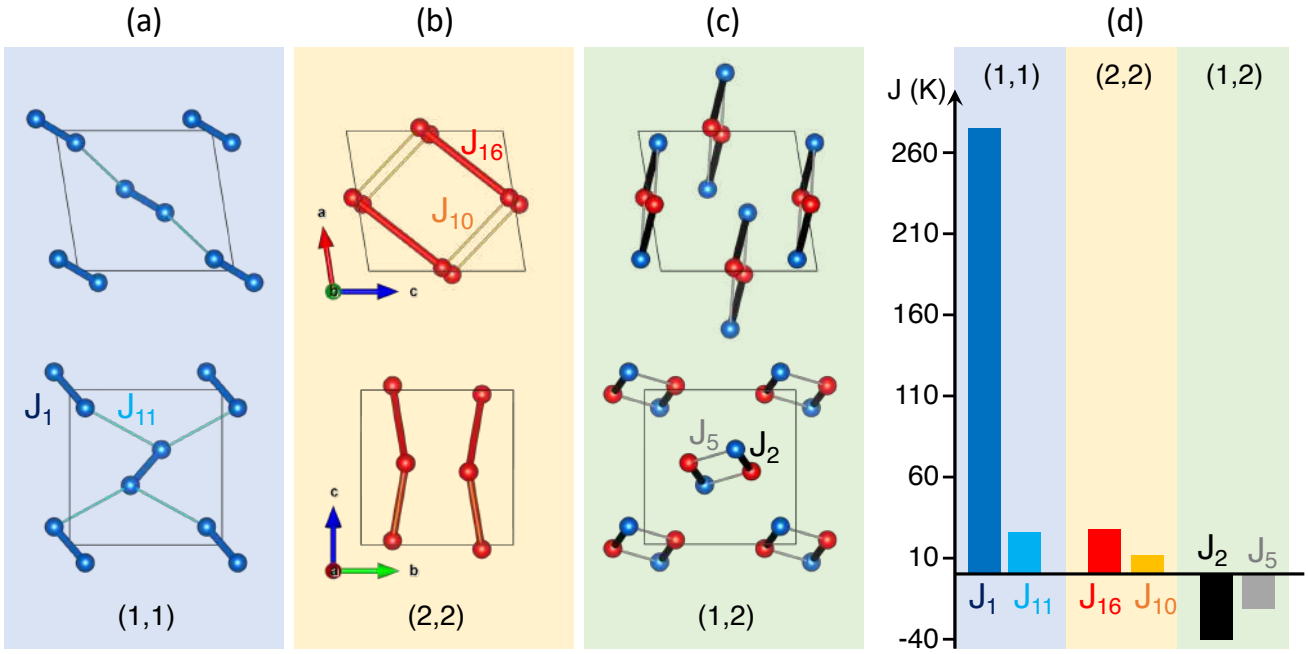

Figure 2. Schematic representation of the predominant J_{ij} exchange couplings, along a (bottom) and b (top) directions, for the Cu(1) subsystem (a) and the Cu(2) subsystem (b) and intercouplings between the Cu(1) and Cu(2) subsystems (c). (d) Comparison of the intensity for magnetic interactions in $SeCuO_3$ estimated from DFT calculations. AFM (FM) couplings are indicated with a positive (negative) sign. The two inequivalent copper atoms Cu(1) and Cu(2) are respectively depicted by blue and red spheres.

(wC+wD). In short, models D and C are only based on one magnetic coupling, respectively J_1 and J_{16}, while models wC and wD use two magnetic interactions each, respectively (J_{16}, J_{10}) and (J_1, J_{11}). In the last model (wC+wD), four magnetic interactions are taken into account (*i.e.* J_{16}, J_{10}, J_1 and J_{11}).

The temperature dependence of the susceptibility tensor, $\hat{\chi}_{\rm D}(T)$, of the spin-1/2 dimer (model D) is given per spin by the following expression taken from Ref. 26

$$\hat{\chi}_{\rm D}(T) = \frac{N_A \mathbf{g}_1 \mathbf{g}_1^T \mu_B^2}{k_B T(3 + exp^{J_1/k_B T})}, \qquad (3)$$

where N_A is the Avogadro constant, $\mathbf{g}_1$ is the Cu(1) g-tensor derived from previously reported ESR measurements made by some of us [7], μ_B is the Bohr magneton, k_B is the Boltzmann constant and J_1 is the intradimer DFT interaction reported in Section III A.

For the isolated spin $S = 1/2$ chain (model C), the temperature dependence of the susceptibility tensor, $\hat{\chi}_C(T)$, was calculated following Ref. 27 with the intrachain interaction J_{16}. Here, the Cu(2) g-tensor $\mathbf{g}_2$ was taken also from our previous study [7].

For the weakly coupled dimer model (wD) the temperature dependence of susceptibilty $\hat{\chi}_{\rm wD}(T)$ is given in Ref. 28 by

$$\hat{\chi}_{\rm wD}(T) = \frac{\hat{\chi}_D(T)}{1 + \frac{2zk_B J_{11}}{N_A \mathbf{g}_1 \mathbf{g}_1^T \mu_B^2} \hat{\chi}_D(T)} \qquad (4)$$

where J_{11} represents the interdimer interaction and z is the number of neighboring coupled dimers through J_{11}. Similar expression can be applied for weakly interacting chains (wC)

$$\hat{\chi}_{\rm wC}(T) = \frac{\hat{\chi}_C(T)}{1 + \frac{2zk_B J_{10}}{N_A \mathbf{g}_2 \mathbf{g}_2^T \mu_B^2} \hat{\chi}_C(T)} \qquad (5)$$

where J_{10} is the interchain interaction and z is now the number of neighboring chains which interact through J_{10}.

In Figure 3, we compare the calculated magnetic susceptibility of the fifth model (wC+wD) with the measured average susceptibility (dotted blue line). In this model, half of the spins are involved in dimers (Eq.(4)) and half in chains (Eq.(5)). Considering that there is no adjustable parameters, except for a slightly smaller value obtained around the maximum, the agreement is excellent. The magnetic susceptibilities of the isolated and weakly interacting dimer, *i.e.* D and wD, are also plotted (red lines), as well as the susceptibility of the isolated and weakly interacting chains, *i.e.* C and wC, (black lines). In both cases, one Cu per mole was assumed (this is equivalent to assuming all spins in dimers, or all spins in chains). While the proposed value of J_{16} gives the maximum of susceptibility at a correct temperature in the isolated chain model C, the magnitude is much larger than the experimental one. We also noticed that the inclusion of the interchain coupling J_{10} (*i.e.* the

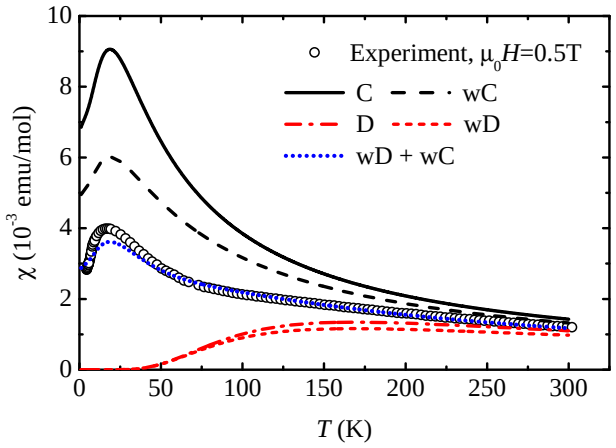

Figure 3. Average experimental magnetic susceptibility *vs* temperature, measured in $\mu_0 H = 0.5$ T, compared to the ones computed from five magnetic models. C, wC, D and wD correspond to isolated chains ($J_{16} = 29.2$ K), weakly-interacting chains ($J_{16} = 29.2$ K and $J_{10} = 12.6$ K), isolated dimers ($J_1 = 270.0$ K) and weakly-interacting dimers ($J_1 = 270.0$ K and $J_{11} = 26.4$ K). The last model wC+wD combines all magnetic couplings of the two subsystems without any intercouplings, *i.e.* J_1, J_{10}, J_{11} and J_{16}.

wC model) cannot remedy that. Using larger interchain interaction would change the effective one-dimensionality of the model since J_{10} is already almost half of J_{16}. Regarding the isolated and weakly interacting dimer models (*i.e.* D and wD), both cases fail to reproduce the strong enhancement of the magnetic susceptibility observed at low temperature, but tend to recover the experimental values for very high temperatures. The direct comparison between (C, wC) and (D, wD) couples of simulations with the experimental data confirms that the presence of AFM chains is a key ingredient for accessing magnetic properties of $SeCuO_3$ at low-temperature.

To complete our analysis, let's consider now the investigation of the magnetic susceptibility anisotropy. Such property was extracted from the measured torque in two planes of measurements as made in Ref. 7

$$\tau_{b,[101]^*} = \frac{mH^2}{2M_{mol}} (\chi_b - \chi_{[101]^*}) \sin(2\theta - 2\theta_b), \qquad (6)$$

$$\tau_{ac} = \frac{mH^2}{2M_{mol}} \Delta\chi_{ac} \sin(2\theta - 2\theta_0), \qquad (7)$$

where $\tau_{b,[101]^*}$ is the torque measured in the plane spanned by the b and $[101]^*$ axes, τ_{ac} is the torque measured in the ac plane, m is the mass of the sample, M_{mol} is the molar mass, H is applied magnetic field, $\chi_b - \chi_{[101]^*}$ is the susceptibility anisotropy in the (b, $[101]^*$) plane, $\Delta\chi_{ac}$ is the susceptibility anisotropy in the ac plane, θ is the goniometer angle, θ_b is the angle at which the field is applied along the b axis and θ_0 is the angle at which the measured torque is zero in the ac plane (see Figure 3 of Ref. [10]) [29]. The angle θ_0 represents the position of one of the susceptibility eigenaxis in the ac plane, while the other is at $\theta_0 + 90°$. The angular dependence of measured torque is a sine curve with a period of 180°, where the amplitude reflects the susceptibility anisotropy. The orientation of macroscopic magnetic eigenaxes can be estimated at points where the torque curve crosses the zero value. The torque curves were calculated for the different models from the susceptibility tensors given above. The magnetic torque is then computed from $\boldsymbol{\tau} = m/M_{mol}\ (\hat{\chi}\mathbf{H}) \times \mathbf{H}$ (m is the mass of the sample, M_{mol} is the molar mass, $\mathbf{H}$ is the applied magnetic field) for each plane of measurement. The resulting anisotropy data obtained for each model are compared to the experimental ones in Figures 4 and 5.

In Figure 4, the sine curves determined for the models involving only chains (*i.e.* C and wC) cross the torque zero value at different angles, in sharp contrast with the models involving only dimers (*i.e.* D and wD). Such behavior is a direct consequence of the different g-tensors of the crystallographically and magnetically inequivalent Cu(1) and Cu(2) that we used in calculations for dimers and chains, respectively, which have different eigenaxes (see $Cu(1)O_4$ and $Cu(2)O_4$ squares in Figure 1). Here, only the wC+wD model gives the correct direction of eigenaxes marked by θ_0 in top panel of Figure 4. The rotation of macroscopic magnetic eigenaxes (θ_0) with temperature, shown in middle panel of Figure 5, is *quantitatively* explained by the wC+wD model (down to $T = 40$ K). We also plot, for comparison, the results for the models C and D, which do not yield rotation of magnetic eigenaxes, as can be seen in middle panel of Figure 5.

Finally, the temperature dependence of magnetic susceptibility anisotropy is quantitatively explained by the model wC+wD (down to 40 K). We notice that for any copper $S = 1/2$ system with isotropic interactions, we expect the susceptibility anisotropy to have the same temperature dependence in the paramagnetic state in any plane of measurement, with only the magnitude being slightly different due to g-factor anisotropy (more details are provided in the Supplementary Materials [30]). This is true for the chains only (*i.e.* C and wC) and dimers only (*i.e.* D and wD) models plotted in top and bottom panels of Figure 5. However, the experiment shows very different behavior in two different crystallographic planes, which is nicely captured by the model wC+wD.

Lastly, we comment on the disagreement between the measured and calculated curves below ~ 40 K, which is mostly apparent for the ac plane. There are two possible reasons that come to mind. The first is the presence of relatively strong FM interactions J_2 and J_5, which we did not take into account in our wC+wD model. The second is the possibility of Dzyaloshinskii-Moriya interaction (DMI) [31] between the spins of the Cu(2) chains, since they are not related by an inversion symmetry center. The DMI is well documented to introduce large anisotropy in the magnetic susceptibility at low temperatures usually below the susceptibility maximum [32], [33], [34].

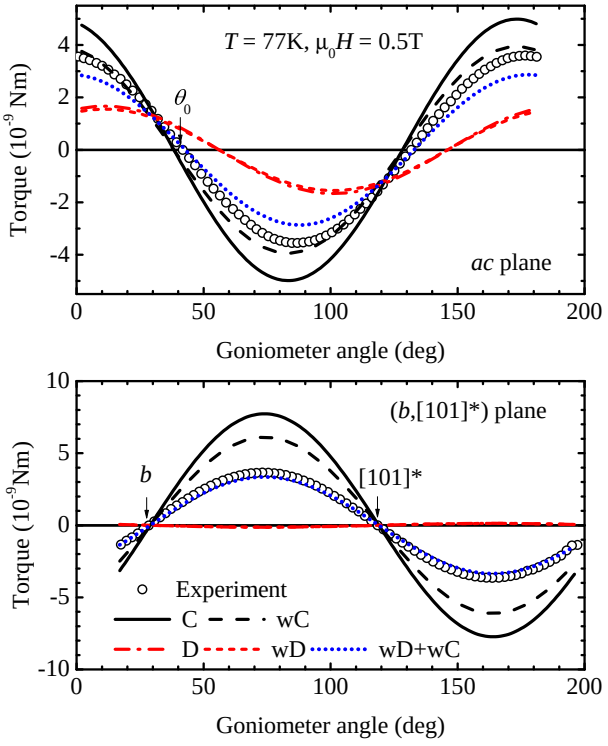

Figure 4. Angular dependence of torque measured at T = 77 K, in $\mu_0 H$ = 0.5 T, in two different planes compared to the C, wC, D, wD and wC+wD models shown by black solid, black dashed, red dashed, red dotted and blue dotted lines, respectively.

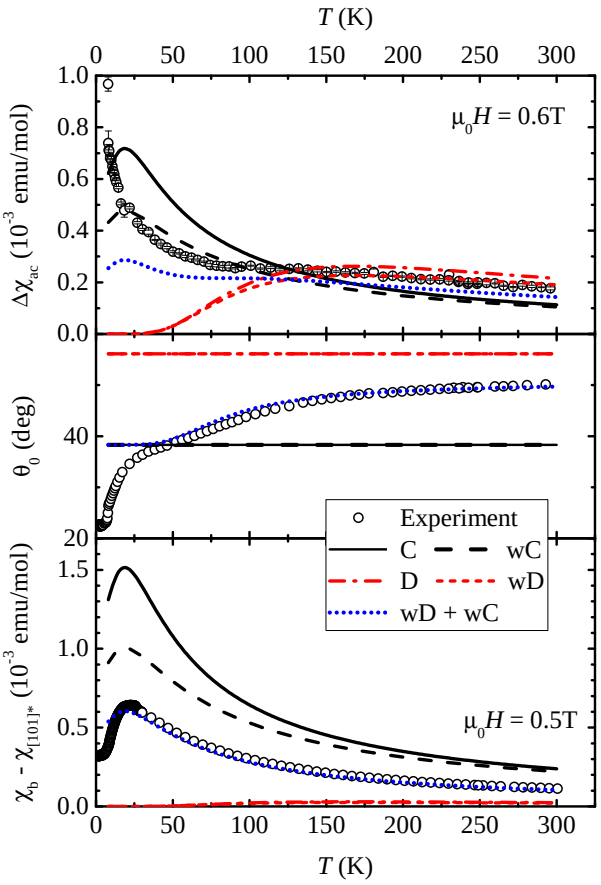

Figure 5. Temperature dependence of susceptibility anisotropy measured in the ac plane and plane spanned by $(b, [101]^*)$ axes (top and bottom panel), in $\mu_0 H$ = 0.6 T and 0.5 T, respectively. Middle panel: Temperature dependence of the torque phase θ_0 which corresponds to the direction of magnetic eigenaxis in the ac plane. The results for C, wC, D, wD and wC+wD models are shown by black solid, black dashed, red dashed, red dotted and blue dotted lines, respectively.

C. Magnetization

The high-field magnetization $M(\mathbf{H})$ of $SeCuO_3$ was measured at 1.4 K for magnetic fields applied along the [010] and [10-1] directions [35], *i.e.* the hard and easy magnetization axes, respectively. The related data are shown respectively by solid black and red lines in Figure 6. In both cases, onsets of half-magnetization plateaus are observed above H_{c1} = 41 and 45 T, for μ_0H parallel to [010] and [10-1], respectively. These values, deduced from the derivative of M(H) (see Figure S5 in Supplementary Materials [30]), are very close to the ones previously reported although it was for magnetic field applied parallel and perpendicular to the [100] direction [8]. It should be emphasized that the AFM chains are along the [10-1] direction (defined by J_{16}), which is also close to the easy magnetization axis (*i.e.* $[\bar{1}01]^*$ direction). As a consequence, a higher magnetic field is needed to reach the plateau when the magnetic field is applied along the [10-1] direction. Such an half-magnetization plateau is the signature that only half of the spins are polarized parallel to the applied field, *i.e.* the Cu(2) spins of the AFM chains. On the other side, the Cu(1) spins of the AFM dimers are still in a singlet state, and a higher field is needed to overcome the singlet-triplet gap, estimated from nuclear quadrupole resonance (NQR) measurements at Δ = 217 ± 7 K [9].

The DMRG results reported in Figure 6a have been obtained using an average g value <g> = 2.191 deduced from ESR measurements [7]. Two plateaus are predicted, with magnetization values of 0.55 and 1.10 μ_B/Cu^{2+}. The first value is in good agreement with the half-magnetization experimental ones, i.e. 0.55 and 0.56 for μ_0H parallel to [10-1] and [010], respectively, validating the use of <g> = 2.191 for our DMRG simulations. It leads to predict that the Cu(2) spins in the dimers would be in the triplet state above 201 T considering isolated dimers model, 222 T when including the inter-dimer and 214 T when adding the dimer-chains interactions, which is in very good agreement with the NQR estimation [9]. Figure 6b provides a closer look of the comparison between the experimental measurements and the DMRG simulations. First of all, the measurements evidenced a S-shape curvature, typical for a spin chain [36]. This fea-

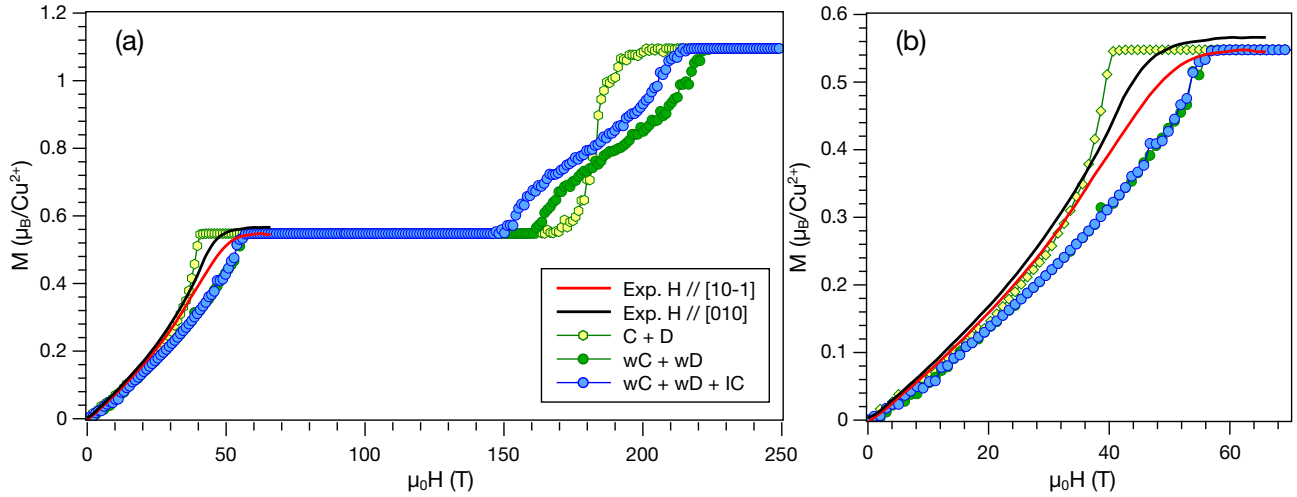

Figure 6. Magnetization *vs* the applied magnetic field H. Experimental data, measured at T = 1.4 K, are represented by red and black curves for H parallel to [10-1] and [010] directions, respectively. The DMRG simulations are represented by yellow, green and blue circles. The theoretical data were obtained using g = 2.191, which corresponds to the average g value reported in [7]. IC refers to the FM intercouplings between the sublattices Cu(1) and Cu(2). DMRG calculations were done using n = 20 for wC+wD and wC+wD+IC and n = 50 for C+D models.

ture is well reproduced by the DMRG simulations. More precisely, our calculations predict $H_{c1} = 41$ T for isolated chains (*i.e.* with only J_{16} couplings in the magnetic model). If we include J_{10}, which is AFM, the critical field is shifted towards higher fields, *i.e.* $H_{c1} = 57$ T. It should be noticed that adding an FM J_{10} would lead to reduce the value of H_{c1}. In addition, the slope of the $M(\mathbf{H})$ curve is too steep with C+D model, while it is very close to the experimental ones when including the inter-chain interactions. It should be noticed that using <g> = 2, leads to larger deviations, *i.e.* gentler slope than experiments and $H_{c1} = 64$ T (see Figure S6 in Supplementary Materials [30]).

The half-magnetization plateau reflects the way the Cu(2) chains (with J_{16} as the main interaction) are polarized by the applied magnetic field. While including the AFM coupling (J_{10}) between the chains displaces the plateau towards higher fields, the inclusion of the FM interactions (J_2 and J_5) between Cu(1) and Cu(2) sublattices has no effect on the half-magnetization plateau. Figure 7a and 7b show the Néel magnetic orders compatible with the leading exchange interactions when the magnetic field is $H < H_{c1}$ and $H_{c1} < H < H_{c2}$, respectively. The effective spin model deduced from our DFT calculations is also given. Figure 7a shows that J_{16} and J_{10} contribute to the energy of the ground state magnetic order (no frustration), while the frustrated J_2 and J_5 interactions do not, explaining the evolution of the magnetization curve at low magnetic fields. For magnetic fields $H > H_{c1}$, the Cu(2) sublattice is fully polarized as shown in Figure 7b. As a consequence, the Cu(2) polarized spins contribute as an additional effective magnetic field through the FM interactions to the applied magnetic field, reinforcing locally the polarization of the Cu(1) dimers. It explains that the inclusion of the FM interactions displaces the second magnetization plateau towards lower fields.

The present magnetization curve, exhibiting two magnetization plateaus, is quite similar to the one reported for $CdCu_2(BO_3)_2$ [37], which consists of two magnetic subsystems, as $SeCuO_3$. For both systems, a spin model based on weakly-interacting Cu(2)-Cu(1)-Cu(1)-Cu(2) tetramers cannot explain all the experimental data. In particular, the M(H) curve of $CdCu_2(BO_3)_2$ were explained using a frustrated quasi-two dimensional magnetic model, analogous to the Shastry-Sutherland spin model [37]. In addition, the non-frustrated interacting spin-1/2 tetramers model used to explain the inelastic neutron scattering data [38], failed to reproduce the magnetization results. Finally, nuclear magnetic resonance and zero-field muon spin relaxation showed the importance of including in the spin model small interactions between the two magnetic subsystems, *i.e.* Cu(1) and Cu(2) [39]. In both systems, a half-step magnetization plateau is observed, corresponding to the polarization of the Cu(2) spins, and a second plateau is predicted at higher field, corresponding to the suppression of the singlet-triplet gap of the Cu(1) spin dimers.

Last but not the least, in the hypothesis that the field-induced BEC could be reached in $SeCuO_3$, we estimate the critical fields and maximum temperature defining the phase diagram dome using the mean-field formula given by [40]

$$g\mu_B H_{c2}^{MFA} = J_{intra} - \frac{zJ_{inter}}{2}, \qquad (8)$$

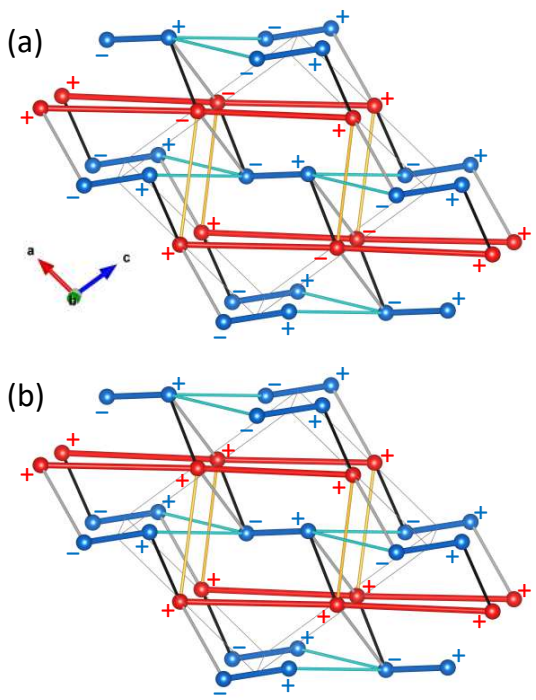

Figure 7. Schematic representation of the effective spin model and magnetic orders in field H < Hc1 (a) and in field Hc1 < H < Hc2 (b). Plus and minus signs indicate up and down spins carried by Cu sites, respectively. The crystallographic unit cell of $SeCuO_3$ is represented by a thin grey line. The J_{ij} exchange couplings are represented using the same color code of Figure 2. The two inequivalent copper atoms Cu(1) and Cu(2) are respectively depicted by blue and red spheres.

$$g\mu_B H_{c3}^{MFA} = J_{intra} + zJ_{inter}, \tag{9}$$

$$T_{max}^{MFA} = \frac{zJ_{inter}}{4k_B}. \tag{10}$$

where J_{intra}, J_{inter} are the intra- and inter-dimer couplings, respectively, and z the number of neighboring dimers. Using $J_{intra} = J_1 = 270$ K, $J_{inter} = J_{11} = 26$ K, $g = 2.191$ and $z = 4$, we obtain $H_{c2}^{MFA} = 148$ T, $H_{c3}^{MFA} = 255$ T and $T_{max}^{MFA} = 26$ K. It is interesting to compare these values with the DMRG results of the wC+wD model yielding $H_{c2}^{wC+wD} = 161$ T and $H_{c3}^{wC+wD} = 222$ T (green circles in Figure 6a). While the agreement is reasonnable between MFA and DMRG results, it remains quite challenging to reach such a BEC regime which requires very high magnetic fields. In addition, T_{max}^{MFA} value is three times larger that the largest reported value for $TlCuCl_3$ [3].

IV. SUMMARY

In summary, we studied the unusual magnetic properties of the low-dimensional *monoclinic*-$SeCuO_3$ compound. Structurally, this material shows tetramer units made by CuO_4 *plaquettes*. Our DFT simulations performed at the PBE+U level demonstrated that $SeCuO_3$ consists of two magnetic subsystems: AFM Cu(1) dimers and AFM Cu(2) spin chains. The two subsystems weakly interact through FM couplings, leading to magnetic frustration. This magnetic model successfully reproduces the magnetic susceptibility and torque magnetometry measurements. Furthermore, our high-magnetic field experiments and DMRG simulations enable us to determine a 1/2-magnetization plateau appearing at 40-45 T and a second plateau at 210-220 T. These two behaviors are respectively associated to the polarization of Cu(2) spin-chains and the switching to the triplet state for Cu(1) dimers.

ACKNOWLEDGMENTS

X. R. and A. S. acknowledge funding from the French National Research agency (ANR - Grant ANR-19-CE08-0013-02; HTHPCM Project). The theoretical work was granted access to the HPC resources of [TGCC/CINES/IDRIS] under the allocation 2020-A0090907682 made by GENCI. X. R., W. L.-D.-H. and M. H. acknowledge support of COGITO project *Theoretical and experimental study of magnetic and multiferroic materials*. M. H. acknowledges support of project Cryogenic Centre at the Institute of Physics - KaCIF (Grant No. KK.01.1.1.02.0012) co-financed by the Croatian Government and the European Union through the European Regional Development Fund - Competitiveness and Cohesion Operational Programme.

[1] A. Vasiliev, O. Volkova, E. Zvereva, and M. Markina, npj Quantum Mater. **3**, 1 (2018).
[2] T. Giamarchi, C. Rüegg, and O. Tchernyshyov, Nat. Phys. **4**, 198 (2008).
[3] V. Zapf, Rev. Mod. Phys. **86**, 563 (2014).
[4] A. Saúl and G. Radtke, Phys. Rev. Lett. **106** (2011).
[5] W. Lafargue-Dit-Hauret, D. Braithwaite, A. D. Huxley, T. Kimura, A. Saúl, and X. Rocquefelte, Phys. Rev. B **103**, 214432 (2021).
[6] I. Živković, D. M. Djokić, M. Herak, D. Pajić, K. Prša, P. Pattison, D. Dominko, Z. Micković, D. Cinčić, L. Forró, H. Berger, and H. M. Rønnow, Phys. Rev. B **86**, 054405 (2012).
[7] M. Herak, A. Grubišić Čabo, D. Žilić, B. Rakvin, K. Salamon, O. Milat, and H. Berger, Phys. Rev. B **89**, 184411 (2014).
[8] S. Lee, W.-J. Lee, J. van Tol, P. L. Kuhns, A. P. Reyes, H. Berger, and K.-Y. Choi, Phys. Rev. B **95**, 054405

(2017).
[9] T. Cvitanić, V. Šurija, K. Prša, O. Zaharko, I. Kupčić, P. Babkevich, M. Frontzek, M. Požek, H. Berger, A. Magrez, H. M. Rønnow, M. S. Grbić, and I. Živković, Phys. Rev. B **98**, 054409 (2018).
[10] N. Novosel, W. Lafargue-Dit-Hauret, Ž. Rapljenović, M. Dragičević, H. Berger, D. Cinčić, X. Rocquefelte, and M. Herak, Phys. Rev. B **99**, 014434 (2019).
[11] L. Testa, V. Šurija, K. Prša, P. Steffens, M. Boehm, P. Bourges, H. Berger, B. Normand, H. M. Rønnow, and I. Živković, Phys. Rev. B **103**, L020409 (2021).
[12] H. Effenberger, Z. Kristallogr. Cryst. Mater. **175**, 61 (1986).
[13] K. Momma and F. Izumi, J. Appl. Crystallogr. **44**, 1272 (2011).
[14] P. Hohenberg and W. Kohn, Phys. Rev. **136**, B864 (1964).
[15] W. Kohn and L. J. Sham, Phys. Rev. **140**, A1133 (1965).
[16] P. Giannozzi, S. Baroni, N. Bonini, M. Calandra, R. Car, C. Cavazzoni, D. Ceresoli, G. L. Chiarotti, M. Cococcioni, I. Dabo, A. D. Corso, S. de Gironcoli, S. Fabris, G. Fratesi, R. Gebauer, U. Gerstmann, C. Gougoussis, A. Kokalj, M. Lazzeri, L. Martin-Samos, N. Marzari, F. Mauri, R. Mazzarello, S. Paolini, A. Pasquarello, L. Paulatto, C. Sbraccia, S. Scandolo, G. Sclauzero, A. P. Seitsonen, A. Smogunov, P. Umari, and R. M. Wentzcovitch, J. Phys. Condens. Matter **21**, 395502 (2009).
[17] J. P. Perdew, K. Burke, and M. Ernzerhof, Phys. Rev. Lett. **77**, 3865 (1996).
[18] K. F. Garrity, J. W. Bennett, K. M. Rabe, and D. Vanderbilt, Comput. Mater. Sci. **81**, 446 (2014).
[19] H. J. Monkhorst and J. D. Pack, Phys. Rev. B **13**, 5188 (1976).
[20] M. Cococcioni and S. de Gironcoli, Phys. Rev. B **71**, 035105 (2005).
[21] C. Wüllen, J. Phys. Chem. A **113**, 11535 (2009).
[22] H. Xiang, C. Lee, H.-J. Koo, X. Gong, and M.-H. Whangbo, Dalton Trans. **42**, 823 (2013).
[23] D. Vaclavkova, A. Delhomme, C. Faugeras, M. Potemski, A. Bogucki, J. Suffczyński, P. Kossacki, A. R. Wildes, B. Grémaud, and A. Saúl, 2D Mater. **7**, 035030 (2020).
[24] A. Saúl, N. Gauthier, R. M. Askari, M. Côté, T. Maris, C. Reber, A. Lannes, D. Luneau, M. Nicklas, J. M. Law, E. L. Green, J. Wosnitza, A. D. Bianchi, and A. Feiguin, Phys. Rev. B **97**, 064414 (2018).
[25] J. Lado, DMRGpy Library. Available at `https://github.com/joselado/dmrgpy`.
[26] B. Bleaney and K. D. Bowers, Proc. Roy. Soc. (London) Ser. A **214**, 451 (1952).
[27] D. C. Johnston, R. K. Kremer, M. Troyer, X. Wang, A. Klümper, S. L. Bud'ko, A. F. Panchula, and P. C. Canfield, Phys. Rev. B **61**, 9558 (2000).
[28] R. L. Carlin and A. J. van Duyneveldt, *Magnetic Properties of Transition Metal Compounds* (Springer-Verlag New York Ink., 1977).
[29] $SeCuO_3$ is monoclinic which means that one of the eigenaxes of the susceptibility tensor is along the b axis, while the other two are in the ac plane [41]. Consequently, the torque will be zero when $H \| b$ which is denoted by angle θ_b in Equation (6), while in the ac plane it will be zero at θ_0 which can be anywhere in the ac plane, and can even change with temperature, which is the case in $SeCuO_3$.
[30] See Supplemental Material at [URL] for more details on temperature dependence of the magnetic susceptibility.
[31] I. Dzyaloshinsky, J. Phys. Chem. Solids **4**, 241 (1958); T. Moriya, Phys. Rev. **120**, 91 (1960).
[32] M. Oshikawa and I. Affleck, Phys. Rev. Lett. **79**, 2883 (1997); I. Affleck and M. Oshikawa, Phys. Rev. B **60**, 1038 (1999); Phys. Rev. B **62**, 9200 (2000).
[33] R. Feyerherm, S. Abens, D. Günther, T. Ishida, M. Meißner, M. Meschke, T. Nogami, and M. Steiner, J. Phys. Condens. Matter **12**, 8495 (2000).
[34] M. Herak, A. Zorko, M. Pregelj, O. Zaharko, G. Posnjak, Z. Jagličić, A. Potočnik, H. Luetkens, J. van Tol, A. Ozarowski, H. Berger, and D. Arčon, Phys. Rev. B **87**, 104413 (2013).
[35] The measurements have been done for a magnetic field along the [10-1] axis, which about 5 degrees close to the reciprocal [-101] direction, which corresponds to the easy magnetization axis.
[36] J. C. Bonner and M. E. Fisher, Phys. Rev. **135**, A640 (1964).
[37] O. Janson, I. Rousochatzakis, A. A. Tsirlin, J. Richter, Y. Skourski, and H. Rosner, Phys. Rev. B **85**, 064404 (2012).
[38] M. Hase, K. Nakajima, S. Ohira-Kawamura, Y. Kawakita, T. Kikuchi, and M. Matsumoto, Phys. Rev. B **92**, 184412 (2015).
[39] W.-J. Lee, S.-H. Do, S. Yoon, Z. H. Jang, B. J. Suh, J. H. Lee, A. P. Reyes, P. L. Kuhns, H. Luetkens, and K.-Y. Choi, Phys. Rev. B **90**, 214416 (2014).
[40] M. Tachiki and T. Yamada, J. Phys. Soc. Jpn. **28**, 1413 (1970).
[41] R. E. Newnham, *Properties of Materials (Anisotropy, Symmetry, Structure)* (Oxford University Press, New York, USA, 2005).